Received 28 February 2021; revised 28 March 2021; accepted 6 April 2021. Date of publication 9 April 2021; date of current version 26 April 2021. The review of this article was arranged by Associate Editor Antonio J. Marques Cardoso.

Digital Object Identifier 10.1109/OJIES.2021.3072232

Sensorless Field-Oriented Control for Open-End Winding Five-Phase Induction Motor With Parameters Estimation

SAAD KHADAR [1,2], HAITHAM ABU-RUB [2] (Fellow, IEEE), AND ABDELLAH KOUZOU [2] (Senior Member, IEEE)

[1] Department of Electrical and Computer Engineering, Texas A&M University at Qatar, Doha, Qatar
[2] LAADI Laboratory, Faculty of Sciences and Technology, Ziane Achour University, Djelfa, Algeria

CORRESPONDING AUTHOR: SAAD KHADAR (saadkhadar@yahoo.com)

This work was supported by Qatar National Library.

ABSTRACT This paper proposes a sensorless field-oriented control (FOC) of an open-end stator winding five-phase induction motor (OESW-FPIM). The FOC technique used is associated with dual Space Vector Modulation (SVM) to provide a constant switching frequency and lower harmonics distortion. Furthermore, a simple hybrid observer is proposed which combines a model reference adaptive system (MRAS) and a sliding mode (SM) observer. The examined observer is designed for the estimation of the rotor flux and rotational speed as well as for the estimation of the load torque disturbances. Lyapunov theorem is used in this paper to prove the observer's stability. The work presented in this paper aims to enhance the researched motor's sensorless control and its robustness against external load disturbances and parameters variation. In the proposed MRAS-SM observer, the reference model is replaced by a SM model which uses a sigmoid function as a switching function to overcome the chattering problem. This combination is intended to make use of the advantages of both strategies. At the same time, to preserve the high-level performance of the sensorless FOC technique and to reduce system uncertainties, an estimation algorithm is developed to identify the rotor resistance and the stator resistance simultaneously during motor operation. The parameter estimation algorithm is combined with the proposed control to improve the speed estimation and control accuracy, particularly at low-speed operation. Finally, the effectiveness of the proposed control is validated in real-time by utilizing a hardware-in-the-loop (HIL) platform.

INDEX TERMS Field-oriented control, five phase induction motor, parameters estimation, MRAS estimator, sensorless control, sliding mode observer.

I. INTRODUCTION

THE past two decades have been marked by increasing research efforts towards developing topologies and control techniques of multilevel inverters and multiphase machines for several industrial applications [1]–[6]. Multilevel inverter topologies have been extensively used for medium and high-power variable speed drives due to their many features such as low voltage stress on power switches, low (dV/dt), lower harmonic distortion in the output voltages, etc., [1]–[4]. There are numerous popular topologies of multilevel inverters. The most used MLIs is the neutral point clamped, the cascaded H-bridge, and the flying capacitor. On the other side, the multi-phase machine drive concepts (more than three phases) are nowadays considered as serious contenders for numerous industrial applications due to their attractive features compared to the three-phase machine such as reduced stator current per phase, reduced rotor harmonic currents, lower torque pulsations, higher torque density, lower MMF harmonics, fault tolerance capability, and higher efficiency [5]–[6]. It is possible to combine the benefits of multi-level inverters and multi-phase machine drives by merely adopting the open-end stator winding (OESW) concept [7]–[9]. Such an approach delivers a multi-level waveform even by feeding the multi-phase machine using dual two-level voltage source inverters (VSI) from both sides of the stator windings [7]. The OESW structure has gained interest due to the offered advantages compared to a standard star or delta-connected solutions. Examples of the advantages are obtaining a multi-level output voltage while using two-level inverters, achieving lower switching frequency operation with enhanced quality. This benefit leads to reduced switching losses, attaining common-mode voltage elimination, and improving fault-tolerant capability [7]–[9]. These features have made OESW variable speed drives with dual-VSI suitable for different high power and emerging applications, such as rolling mills [10], and electric vehicles and hybrid electric vehicles [11]. The concept of OESW topology has been recently applied to systems with a higher number of phases such as five-[7] six-[12], seven-, and nine-phase [13]. Therefore, this concept has motivated the authors to adopt this topology. This paper focuses on the control of an open-end stator winding five-phase induction motor (OESW-FPIM) topology with two separated DC power supplies.

Many control techniques have been used for the OESW-FPIM such as the field-oriented control [14], direct torque control [15], backstepping control [7], and sliding mode control [16]. The FOC technique is an attractive solution due to its simplicity and maturity as it offers high dynamic performance by means of independent torque and flux adjustment within a very wide range of speeds [16], [17]. Unfortunately, FOC technique has the major disadvantage of being sensitive to motor parameters variation and load torque disturbances [17]. This sensitivity may become significant with the commonly implemented untuned proportional integral (PI) controllers. Furthermore, FOC technique requires accurate information on both the rotational speed and the motor flux values. Usually, the rotational speed is obtained with a special encoder (or resolver) placed on the motor shaft or estimated continuously using models or observers. In this regard, speed sensorless control reduces the number of installed sensors, the additional electronic circuits, the connection cables, and the mounting space [7]. Consequently, the overall cost, size, and maintenance requirements are minimized, while the system robustness and reliability are enhanced even when operating in hostile environments [7], [16]. Owing to this, the sensorless control methods have received great attention during the last decades, particularly three-phase motor drives [17]–[24]. Nevertheless, operating the high performance drives in sensorless mode is still facing some persisting challenges, particularly at low speed and under machine parameters variation [18]–[20]. Therefore, the research on multi-phase motor drives under parameters variation is a timely topic and of high importance.

The rotor resistance (R_r) and stator resistance (R_s) values may change up to 100% of their nominal values [25] and, thus, negatively impact the control performance. The estimated flux and speed would deviate from the real values, which deteriorates the drive performance [17]. Therefore, simultaneous estimation of the motor speed and the resistances is required for high performance sensorless FOC drive, especially at low-speed operation.

Lastly, research on simultaneous estimation of rotational speed, rotor resistance R_s and stator resistance R_r has been investigated for obtaining improved motor performance under their variations. Authors in [21] have used a full order adaptive observer algorithm for the estimation of the rotational speed with R_s and/or R_r. However, the used strategies are associated with high computational complexity and introduced poor performance at the instant of parameter variation, particularly in the regenerating mode. In [22], an extended Kalman filter was proposed to estimate the rotational speed and the rotor flux components of the FPIM using current and stator voltage measurements. However, the presented observer requires intensive calculations and proper initialization. Furthermore, the motor parameters were not estimated in this work. In [18], the authors presented a Luenberger observer based on Lyapunov theory to estimate the rotational speed, stator resistance, and some state variables of FPIM drive. However, the used observer is relatively complex, and the gains are sufficiently large to compensate the non-linearity present in the system. In [7] and [24], an MRAS approach was implemented for simultaneous estimation of the rotational speed, rotor resistance, and stator resistance. The MRAS-based techniques of FPIM speed estimation are characterized by their simplicity, but the sensitivity to motor parameters variation is a major problem. In [17], an online estimation method predicated on SM observer has been adopted to simultaneously identify the rotational speed and the rotor resistance of the FPIM. The obtained results have shown the possibility of updating the rotor resistance changes accurately during low-speed operation. However, it has been found that the estimated rotor resistance takes a long time to follow the actual resistance value. In addition, the utilized SM-observer suffers from the chattering phenomenon and is highly influenced by noise. In [24], new schemes based on artificial intelligence (AI) have been used for motor resistances estimation. The acquired results have shown that AI methods are better than classical ones. However, they are more complicated and require training and longer execution time.

Among the presented methods, MRAS-based speed estimation schemes have found widespread application within field-oriented control for motor drives due to their design simplicity and low computational time [7]. Several MRAS-based approaches have been proposed in literature, such as those based on rotor flux error [7], back-electromotive force error [26], stator current error [23], reactive power error [27], and active power error [28]. Therefore, the aim is to present an improvement in the classical MRAS approach using rotor flux sliding mode observer for low-speed operation and under parameters variation.

This paper presents the design and implementation of a robust sensorless control scheme based on MRAS-SM observer. The proposed MRAS-SM observer is used for the simultaneous estimation of the rotational speed, rotor flux, load torque, stator resistance, and rotor time constant (or rotor resistance) for OESW-FPIM. The proposed solution uses only the measured stator currents to the stator terminals. To the best of authors knowledge, this is the first sensorless control solution proposed for the OESW-FPIM topology. The major contributions of the proposed paper can be summarized as follows:

1) A rotor-flux SM-observer approach based on the sigmoid sliding function is proposed. The goal is to avoid the chattering problem. Also, the present work includes a new sliding surfaces quantity to ensure the convergence of the estimated current error to zero in case of the unknown parameters or in case of the application of external perturbations.
2) The estimation of the load torque disturbances based on a mechanical model of the OESW-FPIM topology, which is simpler as opposed to the earlier methods (eg. those presented in [30] and [31]).
3) Proposing an algorithm for the estimation of the stator and rotor resistances. The aim is to achieve high estimation accuracy while reducing the estimation response time and the computational time in comparison with the previous works (eg. those presented in [18]–[21], [23], [26], [27]).
4) An MRAS-SM observer is proposed to ensure the accurate estimation of the rotational speed, rotor flux, stator resistance, and rotor time constant (or rotor resistance) with relatively low computational time in accordance with real-time applications.
5) The proposed control technique is an original solution applied for the first time on the studied motor topology.
6) The paper is organized as follows: Section II introduces the studied OESW-FPIM topology with the dual SVM strategy. The FPIM model is reviewed and details of the FOC technique is presented in Section III. Then Section IV describes the proposed hybrid observer to estimate the rotor speed, the rotor flux, the load torque disturbance, and the motor parameters. The real time simulation and performances evaluation are introduced in Section V. The last section of the paper provides the conclusion of the realized work.

II. DUAL SPACE VECTOR MODULATION

The basic scheme of dual space vector modulation (SVM 1 and SVM 2) used is shown in Fig. 1 [7].

The power circuit of the studied drive is represented in Fig. 2. It comprises of a dual VSI and a FPIM. The studied OESW-FPIM topology is obtained by opening the neutral point of the motor stator windings and supplying it from both terminals by a dual-VSI system (VSI-a and VSI-b), using two separated DC power supplies.

The switching states of both inverters are generated through dual SVM strategy, where the VSI-a pulses are generated in a traditional way and the VSI-b pulses are generated with a 180 degrees phase shift to obtain the maximum voltage applied on the stator windings. According to Kirchhoff's law, the phase voltages of the stator windings are obtained from the

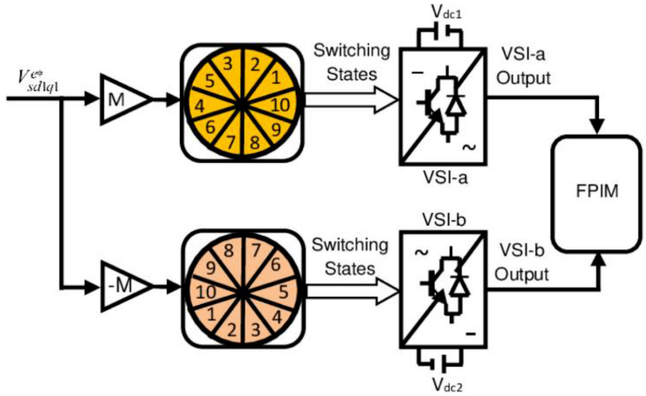

FIG. 1. Dual space vector modulation of OESW-FPIM topology.

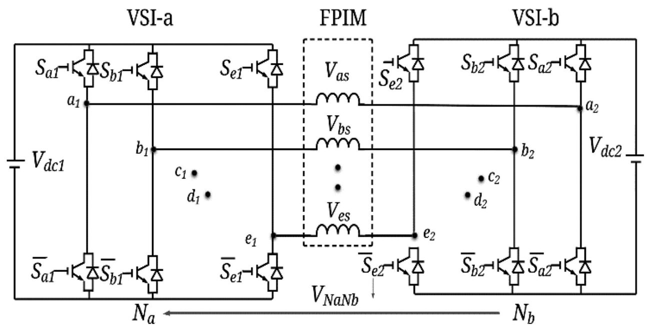

FIG. 2. The power circuit of OESW-FPIM topology.

difference between the inverters output voltages as follows:

$$\begin{bmatrix} V_{as} \\ V_{bs} \\ V_{cs} \\ V_{ds} \\ V_{es} \end{bmatrix} = \frac{1}{5} \begin{bmatrix} 4 & -1 & -1 & -1 & -1 \\ -1 & 4 & -1 & -1 & -1 \\ -1 & -1 & 4 & -1 & -1 \\ -1 & -1 & -1 & 4 & -1 \\ -1 & -1 & -1 & -1 & 4 \end{bmatrix} \begin{bmatrix} V_{a1Na} - V_{a2Nb} \\ V_{b1Na} - V_{b2Nb} \\ V_{c1Na} - V_{c2Nb} \\ V_{d1Na} - V_{d2Nb} \\ V_{e1Na} - V_{e2Nb} \end{bmatrix} \quad (1)$$

The symbols V_{a1Na}, V_{b1Na}, V_{c1Na}, V_{d1Na}, and V_{e1Na} denote the output voltages of the VSI-a. Similarly, the symbols V_{a2Nb}, V_{b2Nb}, V_{c2Nb}, V_{d2Nb}, and V_{e2Nb} denote the output voltages of VSI-b.

Two-level five phase VSI can produce up to $2^5 = 32$ space vectors in each of the frames ($\alpha 1 - \beta 1$ and $\alpha 2 - \beta 2$ frame), as shown in Fig. 3a and Fig. 3b, respectively. There are 30 active vectors and 2 zero vectors. The active vectors can be divided into three groups [7], [15]: Group 1: consists of 10 large magnitude vectors, Group 2: consists of 10 medium magnitude vectors and Group 3: consists of 10 small magnitude vectors. All the active vectors span over 360 degrees in the 2-D plane, forming a decagon with 10 sectors; each with 36 degrees. The decimal numbers that label the space vectors stand for a 5-position binary number. The binary numbers determine the switches states in the five-phase VSI. The voltage vectors in $\alpha 2 - \beta 2$ frame are not involved in the generation of the machine torque [7], [15].

Since a high number of possible switching states (1024) can be performed in the utilized topology, the development of a suitable SVM algorithm becomes a challenge. The basic

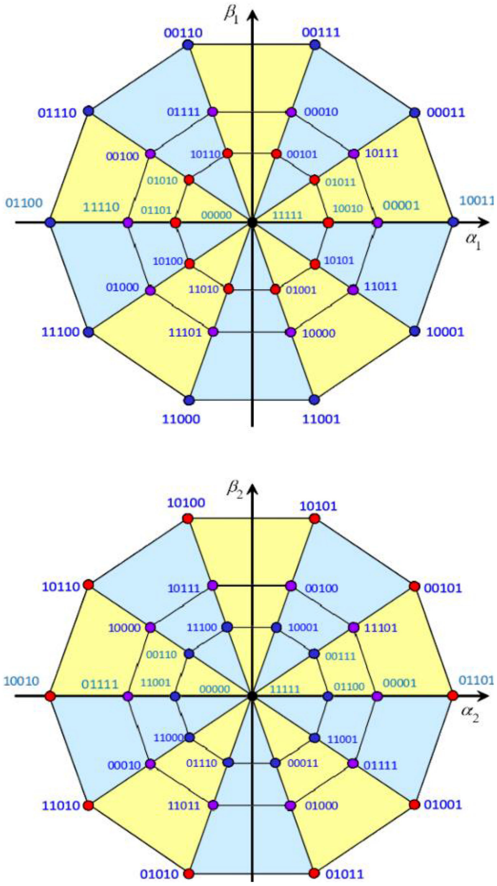

FIG. 3. Space vector combinations in $\alpha 1 - \beta 1 - \alpha 2 - \beta 2$ frame.

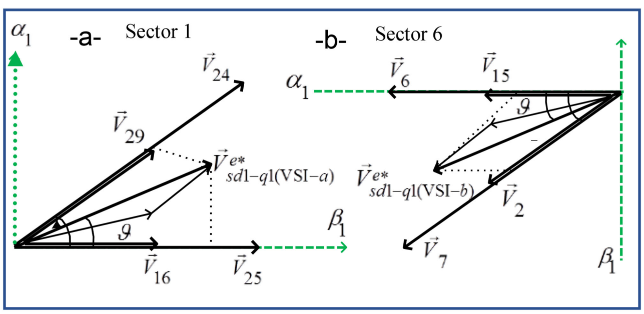

FIG. 4. Principle for SVM-1 and SVM-2.

idea presented in [32] is to decompose the SVM algorithm of the dual-VSI system into two sub systems with lower-level complexity compared with conventional methods [33]. The proposed algorithm in this paper aims to develop a simple SVM strategy that is suitable for the studied OESW-FPIM topology.

The proposed strategy allows for the controlling of the two voltage space vectors independently by splitting the reference $\vec{V}^{e*}_{d1-q1}$ of the dual-VSI system into two reference vectors ($\vec{V}^{e*}_{d1-q1(VSI-a)}$ and $\vec{V}^{e*}_{d1-q1(VSI-b)}$) equally between the two inverters but with opposite directions.

According to Fig. 4, the applied SVM strategy of each inverter is based on the synthesis of $\vec{V}^{e*}_{d1-q1}$ by using the switching times of two large and two medium voltage vectors in each sector. For example, when $\vec{V}^{e*}_{d1-q1(VSI-a)}$ is located in Sector 1, as shown in Fig. 4a, the voltage vector can be synthesized by two adjacent large voltage vectors: $\vec{V}_{25}$ and $\vec{V}_{24}$, two adjacent medium voltage vectors: $\vec{V}_{16}$, $\vec{V}_{29}$ and two zero voltage vectors: $\vec{V}_{30}$ and $\vec{V}_0$. Also, when $\vec{V}^{e*}_{d1-q1(VSI-b)}$ is located in Sector 6, as shown in Fig. 4b, it can be synthesized by two adjacent large voltage vectors: $\vec{V}_6$ and $\vec{V}_7$, two adjacent medium voltage vectors: $\vec{V}_{15}$, $\vec{V}_2$ and two zero voltage vectors: $\vec{V}_{30}$ and $\vec{V}_0$.

III. ROTOR FIELD ORIENTED FPIM MODEL

FOC is the most common used technique in industrial drives, especially for high performance applications [15]. This method's basic goal for the FPIM is to obtain decoupled control of electromagnetic torque and rotor flux by controlling the $d1 - q1$ components of stator currents. If the rotor flux is aligned with the $d1$-axis, then $q1$-rotor flux becomes zero [7], [15], [17]:

$$\begin{cases} \psi_{rd1} = \psi_r \\ \psi_{rq1} = 0 \end{cases} \tag{2}$$

The FPIM model in rotating reference frames ($d1 - q1 - d2 - q2$) can be expressed as follows [7]:

$$\begin{cases} \dfrac{di_{sd1}}{dt} = \alpha_1 i_{sd1} + \omega i_{sq1} + \alpha_2 \psi_r + \dfrac{V_{sd1}}{\sigma L_s} \\ \dfrac{di_{sq1}}{dt} = \alpha_1 i_{sq1} - \omega i_{sd1} + \alpha_2 \psi_r + \dfrac{V_{sq1}}{\sigma L_s} \\ \dfrac{di_{sd2}}{dt} = -\dfrac{R_s}{L_{ls}} i_{sd2} + \dfrac{V_{sd2}}{L_{ls}} \\ \dfrac{di_{sq2}}{dt} = -\dfrac{R_s}{L_{ls}} i_{sq2} + \dfrac{V_{sq2}}{L_{ls}} \end{cases} \tag{3}$$

$$\begin{cases} \dfrac{d\psi_r}{dt} = \dfrac{1}{T_r}(L_m i_{sd1} - \psi_r) \\ \dfrac{d\omega}{dt} = -\dfrac{B}{J}\omega + \dfrac{T_{em}}{J} - \dfrac{T_L}{J} \end{cases} \tag{4}$$

where, V_{sd1}, V_{sq1}, V_{sd2}, and V_{sq2} are the stator voltage components; i_{sd1}, i_{sq1}, i_{sd2}, and i_{sq2} are the stator current components; ψ_r is the rotor flux component; R_s and R_r are the stator and rotor resistances; L_s, L_r are the stator and rotor inductances; L_{ls}, L_{lr} are the stator and rotor leakage inductances; L_m is the magnetizing inductance; ω is the rotational speed; T_L is the load torque; n_p is the pole pairs number; J is the inertia moment; B is the friction coefficient and d/dt is the derivative operator. Also,

$$\alpha_1 = \frac{1}{\sigma L_s}\left(R_s + \frac{L_m^2 R_r}{L_r^2}\right), \alpha_2 = \frac{R_r L_m}{\sigma L_s L_r}.$$

where, $\sigma = 1 - L_m^2/L_r L_s$ is the dispersion coefficient. The expressions of electromagnetic torque and slip angular speed

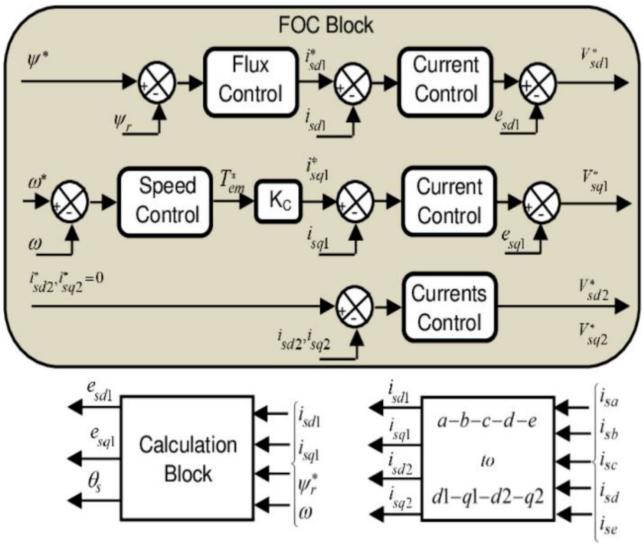

FIG. 5. **FOC technique scheme of FPIM drive.**

of FPIM can be written as follows:

$$\begin{cases} T_{em} = \frac{5}{2}\frac{n_p L_m}{L_r}\psi_r i_{sq1} \\ \omega_{sl} = L_m \frac{i_{sd1}}{T_r.\psi_r} \end{cases} \quad (5)$$

The reference vector angle position (θ_s) which is used for direct or inverse Park transformation is obtained as:

$$\left\{ \frac{d\theta_s}{dt} = \omega + \omega_{sl} = \omega + L_m \frac{i_{sd1}}{T_r.\psi_r} \right. \quad (6)$$

Fig. 5 presents the FOC technique scheme of the FPIM. The main components of this technique are the four control loops (PI controllers are used for all the control loops) and the calculation block. The output of the speed PI controller is the reference torque. The terms e_{sd1} ande_{sq1} presented in the Fig. 5 are expressed as follows:

$$\begin{cases} e_{sd1} = \omega_s \sigma L_s i_{sq1} \\ e_{sq1} = -\omega_s \left(\sigma L_s i_{sd1} + \frac{L_m}{L_r}\psi_r\right) \end{cases} \quad (7)$$

Where, $\omega^*$is the reference speed, $\psi_r^*$is the reference rotor flux and $\psi_r$is the rotor flux.

IV. MRAS-SLIDING MODE OBSERVER

In this section, a robust MRAS-Sliding mode observer based on Lyapunov theory is designed to estimate the rotor flux, rotational speed, and load torque disturbance, using the measured stator currents and supplied voltages. Furthermore, for the enhancement of the system robustness, an estimation of the stator and rotor resistances is proposed.

A. ROTOR SPEED AND ROTOR FLUX ESTIMATION

The conventional structures of MRAS approach is characterized with simple implementation and design flexibility [7], [26]–[28]. However, the sensitivity to the variations of motor parameters at low-speed operation is significant, which is a major disadvantage of using MRAS approach [7], [26]–[28].

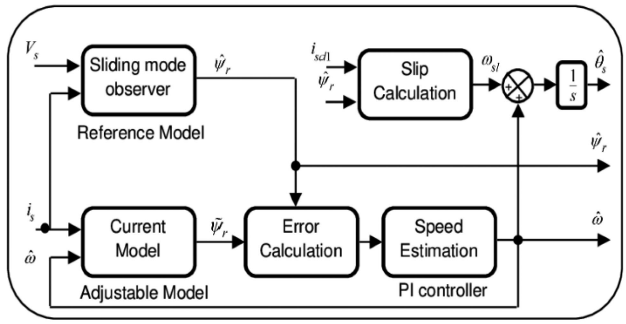

FIG. 6. **The basic principle of proposed MRAS-SM observer.**

To mitigate this problem, a SM observer is proposed in this paper as part of the designed MRAS control approach. The main goal is to obtain accurate rotor flux and speed estimation. The proposed modification is based on using the SM observer as a reference model in MRAS, as shown in Fig. 6.

The dynamic model of the FPIM can be expressed in the stationary $\alpha 1 - \beta 1$ frame, in terms of the stator current and stator flux as follows:

$$\begin{cases} \frac{di^e_{sd1}}{dt} = -\alpha_1 i^e_{sd1} + \frac{\alpha_2\psi^e_{rd1}}{T_r} + \alpha_2\psi^e_{rq1} + \frac{V^e_{sd1}}{\sigma L_s} \\ \frac{di^e_{sq1}}{dt} = -\alpha_1 i^e_{sq1} + \frac{\alpha_2\psi^e_{rq1}}{T_r} - \alpha_2\psi^e_{rd1} + \frac{V^e_{sq1}}{\sigma L_s} \end{cases} \quad (8)$$

$$\begin{cases} \frac{d\psi^e_{rd1}}{dt} = \frac{1}{T_r}(L_m i^e_{rd1} - \psi^e_{rd1}) - \omega\psi^e_{rq1} \\ \frac{d\psi^e_{rq1}}{dt} = \frac{1}{T_r}(L_m i^e_{rq1} - \psi^e_{rq1}) + \omega\psi^e_{rd1} \end{cases} \quad (9)$$

The expressions of the electromagnetic torque of the FPIM can be written as:

$$T_{em} = \frac{5}{2}\frac{n_p L_m}{L_r}\left(\psi^e_{rd1} i^e_{rq1} - \psi^e_{rq1} i^e_{rd1}\right) \quad (10)$$

The SM observer helps to increase the MRAS robustness in the event of parameters variation and internal system noises. However, this observer suffers from the chattering phenomenon due to the use of the signum function [18], [29]–[31]. To eliminate the effect of such an undesirable phenomenon, the classical signum function is replaced in this paper by the next function:

$$sigm(S) = \left(\frac{2}{1 + e^{-\mu S}}\right) - 1 \quad (11)$$

where, μ is a small positive constant. The MRAS-SM observer is composed of three parts:

1) REFERENCE MODEL

The proposed reference model based on SM observer ensures simultaneous estimation of the stator flux and the stator current is constructed as follows:

$$\begin{cases} \frac{d\hat{i}_s}{dt} = -\left(\frac{1}{\sigma T_s} + \frac{1}{\sigma T_r}\right) i_s + \frac{1}{\sigma L_s T_r}\hat{\psi}_s + \frac{V_s}{\sigma L_s} K'' sigm(S) \\ \frac{d\hat{\psi}_s}{dt} = V_s - R_s i_s - K'' sigm(S) \end{cases} \quad (12)$$

Hence, the estimated rotor flux can be calculated as follows:

$$\begin{cases} \frac{d\hat{\psi}^e_{rd1}}{dt} = \frac{L_r}{L_m}\left(\hat{\psi}^e_{sd1} - \sigma L_s \frac{di^e_{sd1}}{d}\right) \\ \frac{d\hat{\psi}^e_{rq1}}{dt} = \frac{L_r}{L_m}\left(\hat{\psi}^e_{sq1} - \sigma L_s \frac{di^e_{sq1}}{d}\right) \end{cases} \tag{13}$$

where, $T_s$is the stator time constant, $T_r$is the rotor time constant, " ^ " denotes the estimation values, and sign represents the *signum* function, V_s, i_s, $\hat{\psi}_s$ and $\hat{\psi}_r$are the stator voltage, stator current, stator flux, and rotor flux in the $\alpha 1 - \beta 1$ frame, respectively.

The sliding mode surface is represented as follows:

$$S = \left[S_{sd1}\ S_{sq1}\right]^T \tag{14}$$

To eliminate the static errors in case of the unknown parameters or in case of the application of external perturbations, a new sliding surface is proposed in this paper, which is designed to force the estimation errors to asymptotically approach zero. These surfaces are defined as:

$$\begin{cases} S_{sd1} = \frac{e_{id}}{\int e_{id}.dt} \\ S_{sq1} = \frac{e_{iq}}{\int e_{iq}.dt} \end{cases} \tag{15}$$

The estimation errors of stator current are defined as:

$$\begin{cases} e_{id} = \hat{i}^e_{sd1} - i^e_{sd1} \\ e_{iq} = \hat{i}^e_{sq1} - i^e_{sq1} \end{cases} \tag{16}$$

where, $k''$is the correction gain, which represents the amplitudes of the control quantities and are determined from the condition of existence of the sliding mode $[\dot{S}_{sd1}\dot{S}_{sq1}]^T \prec 0$.

2) ADJUSTABLE MODEL

The stator flux components can be constructed from the adaptive model as follows:

$$\begin{cases} \frac{d\tilde{\psi}^e_{rd1}}{dt} = \frac{1}{T_r}\left(L_m i^e_{sd1} - \tilde{\psi}^e_{rd1}\right) - \omega\tilde{\psi}^e_{rq1} \\ \frac{d\tilde{\psi}^e_{rq1}}{dt} = \frac{1}{T_r}\left(L_m i^e_{sq1} - \tilde{\psi}^e_{rq1}\right) + \omega\tilde{\psi}^e_{rd1} \end{cases} \tag{17}$$

The error signal between the two models can be expressed as follows:

$$\begin{cases} e_{\psi d} = \tilde{\psi}^e_{rd1} - \hat{\psi}^e_{rd1} \\ e_{\psi q} = \tilde{\psi}^e_{rq1} - \hat{\psi}^e_{rq1} \end{cases} \tag{18}$$

After deriving (18), the error signal derivatives can be obtained as follows:

$$\begin{cases} \dot{e}_{\psi d} = -\frac{e_{\psi d}}{T_r} - \omega\tilde{\psi}^e_{rq1} + \hat{\omega}\hat{\psi}^e_{rq1} \\ \dot{e}_{\psi q} = -\frac{e_{\psi q}}{T_r} + \omega\tilde{\psi}^e_{rd1} - \hat{\omega}\hat{\psi}^e_{rd1} \end{cases} \tag{19}$$

where, $\hat{\omega}$ is the estimated rotational speed. Using (18) and (19), the derivative of the error signal can be written as follows:

$$\begin{cases} \dot{e}_{\psi d} = -\frac{e_{\psi d}}{T_r} - \tilde{\omega}\tilde{\psi}^e_{rq1} - \hat{\omega}.e_{\psi q} \\ \dot{e}_{\psi q} = -\frac{e_{\psi q}}{T_r} + \tilde{\omega}\tilde{\psi}^e_{rd1} + \hat{\omega}.e_{\psi d} \end{cases} \tag{20}$$

where, $\tilde{\omega} = \omega - \hat{\omega}$ is the error signal between the real rotational speed and the estimated rotational speed.

To ensure the stability of the proposed observer, a Lyapunov candidate function is proposed as next:

$$V_L = \frac{1}{2}e^2_{\psi d} + \frac{1}{2}e^2_{\psi q} + \frac{\tilde{\omega}^2}{2.\Gamma} \tag{21}$$

where, Γ is a positive design constant. The derivative of the Lyapunov candidate function can be obtained as next:

$$\dot{V}_L = \dot{e}_{\psi d}.e_{\psi d} + \dot{e}_{\psi q}.e_{\psi q} + \frac{\dot{\tilde{\omega}}.\tilde{\omega}}{\Gamma} \tag{22}$$

Using (20), equation (22) yields to:

$$\dot{V}_L = -\frac{1}{T_r}(e^2_{\psi d} + e^2_{\psi q}) + \tilde{\omega}\left[\frac{\dot{\tilde{\omega}}}{\Gamma} + e_{\psi q}.\tilde{\psi}^e_{rd1} - e_{\psi d}.\tilde{\psi}^e_{rq1}\right] \tag{23}$$

In order to guarantee the observer stability, the time derivative of the Lyapunov candidate function must be negative [7]. This condition can be met if the following equation is verified:

$$\left[\frac{\dot{\tilde{\omega}}}{\Gamma} + e_{\psi q}.\tilde{\psi}^e_{rd1} - e_{\psi d}.\tilde{\psi}^e_{rq1}\right] = 0 \tag{24}$$

Which means:

$$\dot{V}_L = -\frac{1}{T_r}(e^2_{\psi d} + e^2_{\psi q}) \prec 0 \tag{25}$$

In steady state, the rotational speed is constant which leads to $\dot{\tilde{\omega}} = -\dot{\hat{\omega}}$. Form equation (24), the derivative of the estimated rotor speed can be obtained:

$$\frac{\dot{\hat{\omega}}}{\Gamma} = \left[e_{\psi q}.\tilde{\psi}^e_{rd1} - e_{\psi d}.\tilde{\psi}^e_{rq1}\right] \tag{26}$$

Thus, the adaptation mechanism which ensures the stability of the MRAS-SM observer is obtained as follows:

$$\hat{\omega} = \Gamma\int\left[e_{\psi q}.\tilde{\psi}^e_{rd1} - e_{\psi d}.\tilde{\psi}^e_{rq1}\right].dt \tag{27}$$

3) ADAPTATION MECHANISM

To decrease response time and ensure a null steady state error, a PI controller is used for the estimation of the rotational speed based on (26):

$$\hat{\omega} = K_{P\omega}\left[e_{\psi q}.\tilde{\psi}^e_{rd1} - e_{\psi d}.\tilde{\psi}^e_{rq1}\right] + K_{I\omega}\int\left[e_{\psi q}.\tilde{\psi}^e_{rd1} - e_{\psi d}.\tilde{\psi}^e_{rq1}\right] \tag{28}$$

Where, $K_{p\omega}$ and $K_{I\omega}$ are the integral and proportional parameters of the PI speed controller.

B. LOAD TORQUE DISTURBANCE OBSERVER

The proposed sensorless FOC technique requires information on the load torque applied on the motor. Mostly, the load torque is considered as an external disturbance that can be measured directly by a mechanical sensor which increases the system cost and sensitivity to noise. In this paper, a load torque observer based on the motor mechanical equation is proposed to avoid the use of the mechanical sensor and to

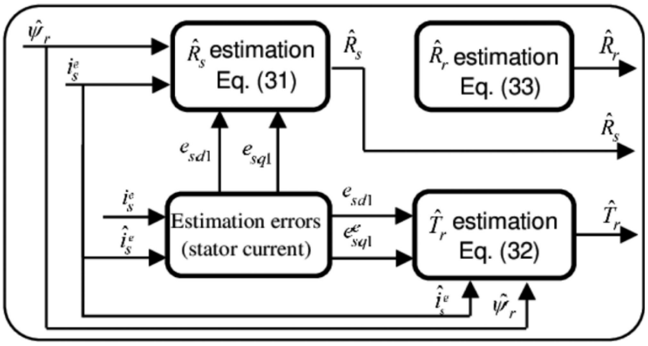

FIG. 7. **The basic principle of the resistance's estimation.**

increase system's robustness [7], [30]. Using (4), (26), the next is obtained:

$$\frac{\hat{T}_L}{J} = \frac{\hat{T}_{em}}{J} - \Gamma\left[e_{\psi q}.\tilde{\psi}_{rd1}^e - e_{\psi d}.\tilde{\psi}_{rq1}^e\right]\left(1+\frac{B}{J}\right) \quad (29)$$

By considering the motion equation of the studied OESW-FPIM topology (4), it is possible to describe the load torque disturbance by using the estimated stator flux and the estimated rotational speed. Thus, the applied load torque can be estimated as follows:

$$\hat{T}_L = \frac{1}{1+\tau_0 P}\left[\hat{T}_{em} - K_{TL}\left[e_{\psi q}.\tilde{\psi}_{rd1}^e - e_{\psi d}.\tilde{\psi}_{rq1}^e\right]\right] \quad (30)$$

where, $\hat{T}_L$ is the estimated load torque, τ_0 is the time constant. $K_{TL}$is arbitrary positive gain.

C. MOTOR PARAMETER ESTIMATION

The most significant disturbances that affect the accuracy of MRAS-SM observer and the performance of the FOC technique are the motor parameters variations. In practice, the motor resistances vary with the change of the temperature which means stator resistance R_s and the rotor resistance R_r deviate from their nominal values or initial values, as it is shown clearly in (12), $R_s$value has important role in the reference model therefore its value should be known with good precision to obtain an accurate estimation of the stator flux components. In the same context, the FOC technique is dependent on the rotor parameters ($R_r$or T_r) [34]. Therefore, any deviation of the rotor parameters between the actual values and the values used in the controller, leads to the wrong estimation of the rotor position and rotational speed and consequently causing poor control and possibly unstable operation of the motor, especially at low-speed operation. To overcome these problems and to improve the robustness and the accuracy of the MRAS-SM observer, an approach is designed in this paper to estimate the $R_s$and $R_r$for the MRAS-SM observer and at the same time improve the performance of the sensorless FOC technique in the presence of motor parameters uncertainty within a wide range of speed operations. The basic principle of the resistance parameter estimation is shown in Fig. 7. The stator resistance estimation is obtained as follows: [35]:

$$\hat{R}_s = \hat{R}_{s0} - K_{Rs}\int\left(\hat{\psi}_{rd1}.\hat{e}_{sq1} - \hat{\psi}_{rq1}.\hat{e}_{sd1}\right)dt \quad (31)$$

where, $K_{Rs} = \chi a/\sigma L_s$ is the estimation gain, χa is a positive correction and R_{s0} is the initial value of the R_s. Similarly, the rotor time constant can be estimated as follows [36]:

$$\frac{1}{\hat{T}_r} = K_{Tr}\int\left(\hat{e}_{sd1}\left(\hat{\psi}_{rd1} - L_m\hat{i}_{sd1}\right) + \hat{e}_{sq1}\left(\hat{\psi}_{rq1} - L_m\hat{i}_{sq1}\right)\right)dt \quad (32)$$

The final equation for the rotor resistance estimation as:

$$\hat{R}_r = \frac{K_{Tr}}{L_r}\int\left(\hat{e}_{sd1}\left(\hat{\psi}_{rd1} - L_m\hat{i}_{sd1}\right) + e_{sq1}\left(\hat{\psi}_{rq1} - L_m\hat{i}_{sq1}\right)\right)dt \quad (33)$$

where, K_{Tr} is a positive correction. The estimation errors of stator currents can be obtained as follows:

$$\begin{cases} \hat{e}_{sd1} = i_{sd1} - \hat{i}_{sd1} \\ \hat{e}_{sq1} = i_{sq1} - \hat{i}_{sq1} \end{cases} \quad (34)$$

V. RESULTS AND ANALYSES

The advantages of the proposed sensorless control of the FPIM-OESW and the estimation accuracy of MRAS-sliding mode observer presented in this paper is verified through hardware-in-the-loop in a real time platform. The reference rotor flux is set to 0.8 Wb. The electrical and mechanical parameters of the motor are as follows: $P = 2.2\,\mathrm{kW}$, $R_s = 2.9\,\Omega$, $R_r = 2.7\,\Omega$, $L_s = 796.4\,\mathrm{mH}$, $L_r = 796.4\,\mathrm{mH}$, $L_m = 785.2\,\mathrm{mH}$, $J = 0.007\mathrm{Kg.m}^2$, $B = 0.0018\mathrm{N.m.s}$, and $n_p = 1$. The inverters switching frequency is set to 5 kHz. The sampling time is $50\mu s$. The arbitrary positive gain is Γ=150. The estimator time constant is τ_0=0.05s.

The gains of flux controller are $K_{p\psi}$=13 and $K_{i\psi}$=45. The gains of speed controller K_{pt}=2 and K_{it}=40. The gains of current controllers K_{pd1}=2500, K_{id1}=225, K_{pq1}=2500, K_{iq1}=225, K_{pd2}=1000, K_{id2}=200, K_{pq2}=1000 and K_{iq2}=200. The gains of PI controller for rotational speed estimation are $K_{i\omega}$= 100 and $K_{p\omega}$=900.

A. HARDWARE-IN-THE-LOOP DESIGN

Hardware-in-the-loop (HIL) methodologies have widely attracted attention in recent years within the field of power electronics and drives as a fast and reliable way to verify the control system [36], [37]. The HIL platform is a good and credible solution for early real-time testing of control systems before their full implementation on actual processes. In this paper, the dual inverter system and the FPIM drive are modeled on OPAL-RT simulator (OP5600), while the proposed control system is implemented on a dSpace platform (DSP-1103) board. Such structure presents a HIL solution for

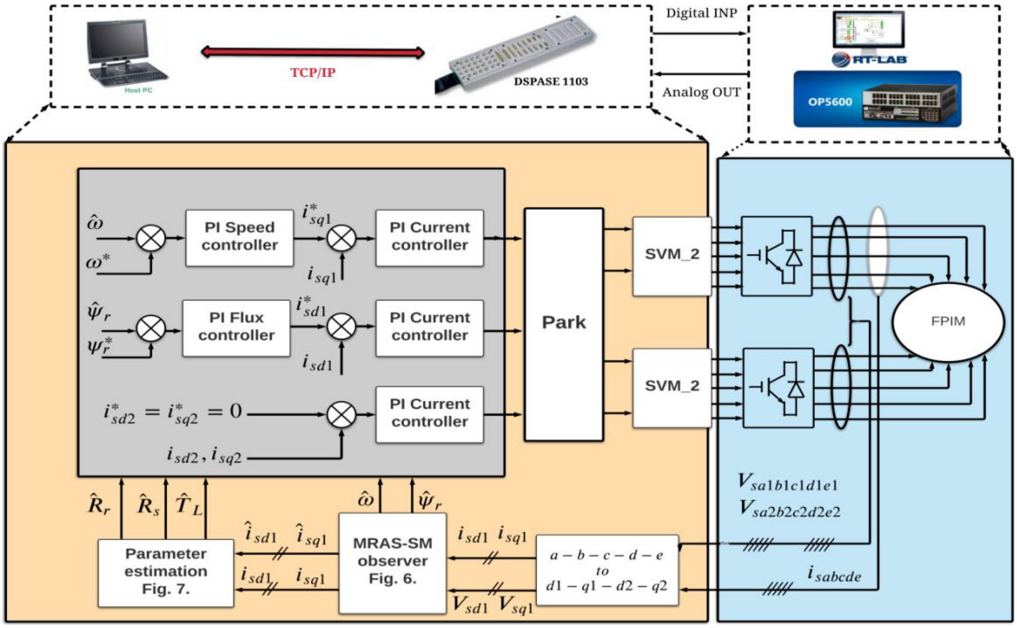

FIG. 8. **The structure of hardware-in-the-loop for the overall control system of the studied topology.**

the overall control system as shown in Fig. 8. The control algorithm is implemented in real time using DSP-1103 board to generate the switching states of the dual inverter system. The switching states are captured by FPGA-based digital input card, which sends the control signals to the two inverters which are implemented on the Opal-RT simulator. Then the feedback signals, such as stator currents and stator voltages, are generated by OP6500 and sent to the DSP board through analog boards.

B. LOAD TORQUE VARIATION

The first conducted test is performed to verify the performance of the proposed control algorithm with the estimation of the load torque disturbances and the motor resistances. The reference speed, rotational speed, and estimated speed of the studied motor are shown in Fig. 9. It is clear that the estimated speed tracks the actual rotational speed well according to the reference speed. The error between the rotational speed and the estimated speed is shown in Fig. 10. This error is close to zero during the steady state operation and with very small increase at the instants of load torque change. In fact, the estimation error is significantly decreased compared to the results presented in [3], [29] and [38]. Thus, the proposed MRAS-SM observer offers precise estimation and high dynamics response.

On the other side, the estimated load torque, obtained from the load torque observer is compared with the reference load torque as shown in Fig. 11. It is obvious that the estimated load torque tracks accurately the imposed reference load torque which proves the effectiveness of the proposed solution. Fig. 12 shows the electromagnetic torque and load torque disturbance. It can be observed that the developed torque presents fast and accurate dynamics after load torque

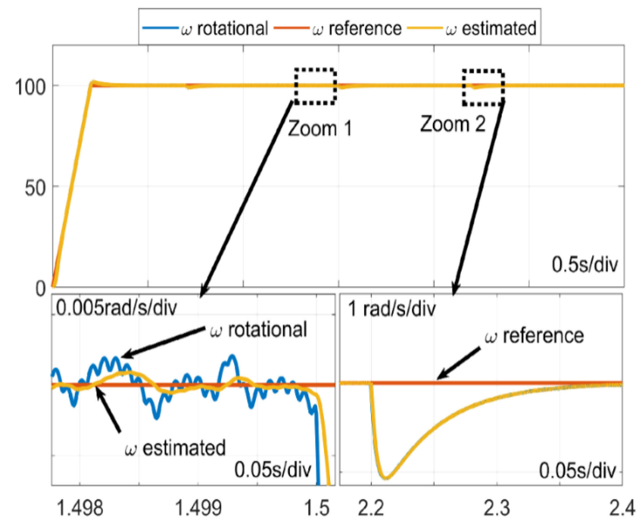

FIG. 9. **The reference, rotational, and estimated speed.**

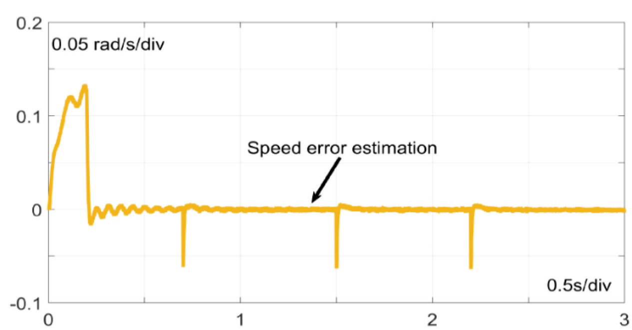

FIG. 10. **The speed estimation error.**

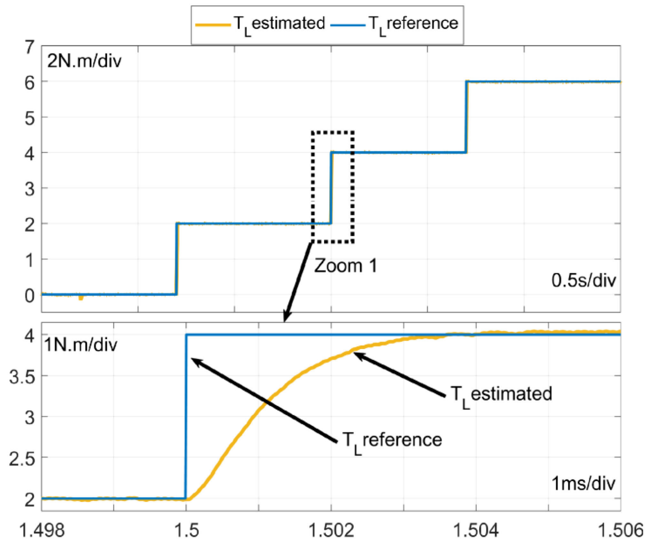

FIG. 11. **The estimated load torque with reference load torque.**

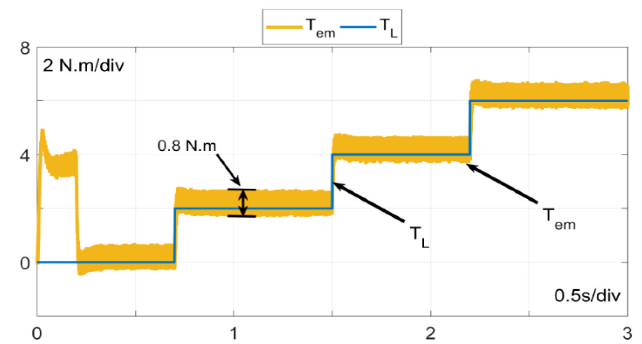

FIG. 12. **The developed electromagnetic torque with applied load torque.**

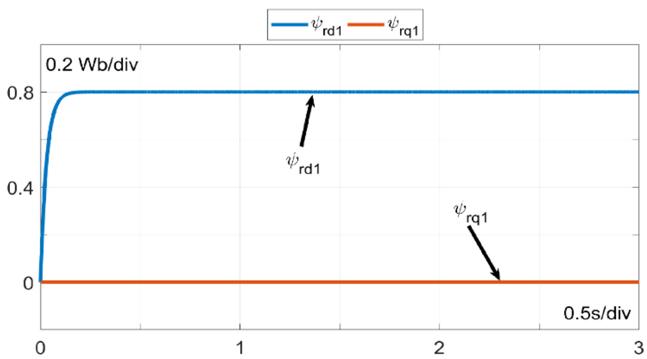

FIG. 13. **The d1-q1 rotor flux components in the synchronous frame.**

changes and with acceptable torque ripples compared to the results presented in many earlier works such as in [3], [18], [23], [38]–[41].

Fig. 13 presents the rotor flux components in the $d1-q1$ rotating frame. It can be noticed that q1-rotor flux is almost zero, while the d1-rotor flux is stabilized at the reference flux (0.8 Wb). This result proves that the full decoupling between the rotor flux and developed electromagnetic torque is maintained.

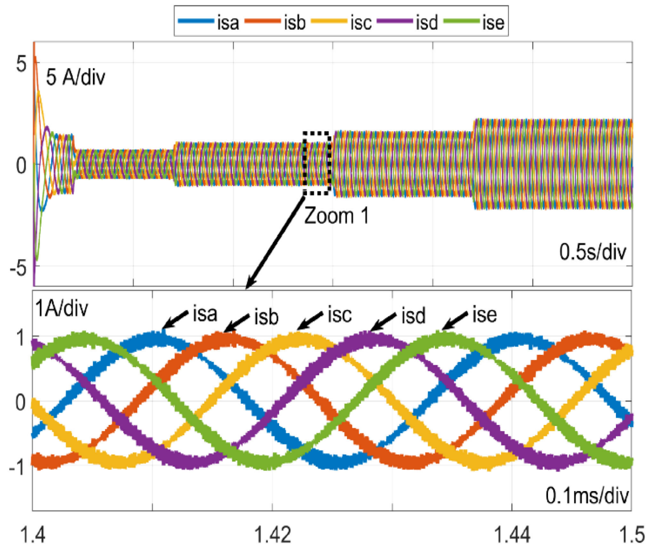

FIG. 14. **The five phase stator currents.**

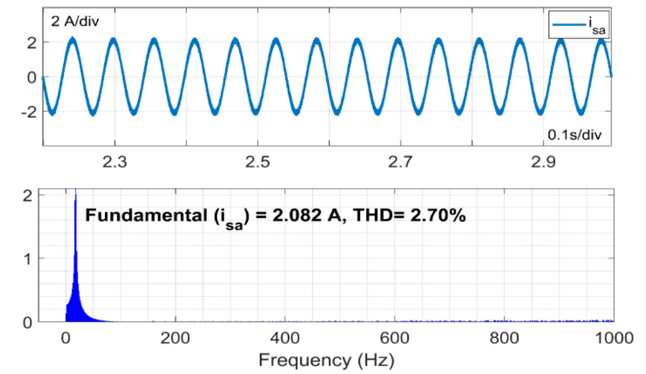

FIG. 15. **The first phase stator current and its harmonic spectrum.**

Fig. 14 shows that the five-phase stator currents have a balanced sinusoidal waveform with reduced chattering compared to the chattering observed in previous works [30], [40], [40]. The phase stator current and its harmonic spectrum are shown in Fig. 15. Current's total harmonic distortion (THD) is 2.70% which is nearly 60% compared to the THD obtained with other techniques such as those presented previously in [3], [39], [42].

On the other side, the estimated resistances of the rotor and stator windings are shown in Fig. 16. It is evident that the proposed estimation algorithm allows accurate motor parameters estimation. Furthermore, the load torque variation has no influence on the estimation performance compared to the works presented in [19], [38].

C. ROBUSTNESS TEST

In this test, the studied motor is tested at a low speed of 10 rad/s with constant load torque. In order to study the effect of the motor parameters variation on the performance of the speed estimation, the motor is started with its initial stator resistance value $R_s = 2.9\Omega$, and after 1.5s, $R_s$is changed to

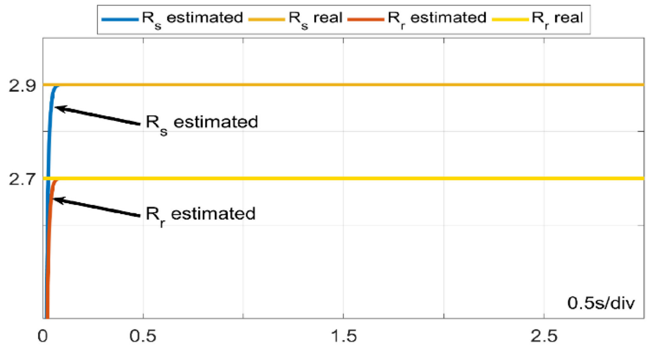

FIG. 16. The estimated resistances of rotor and stator windings.

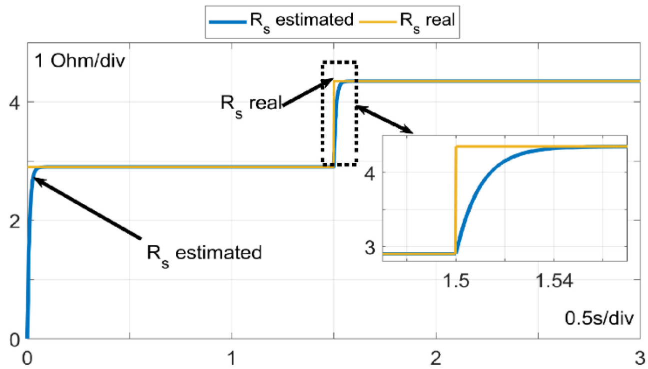

FIG. 17. The estimated and real rotor resistance.

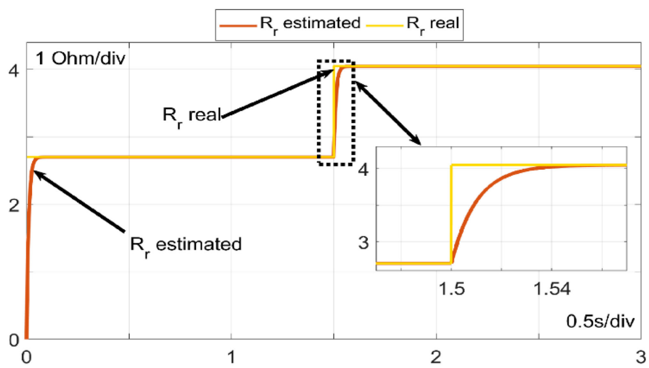

FIG. 18. The estimated and actual stator resistance.

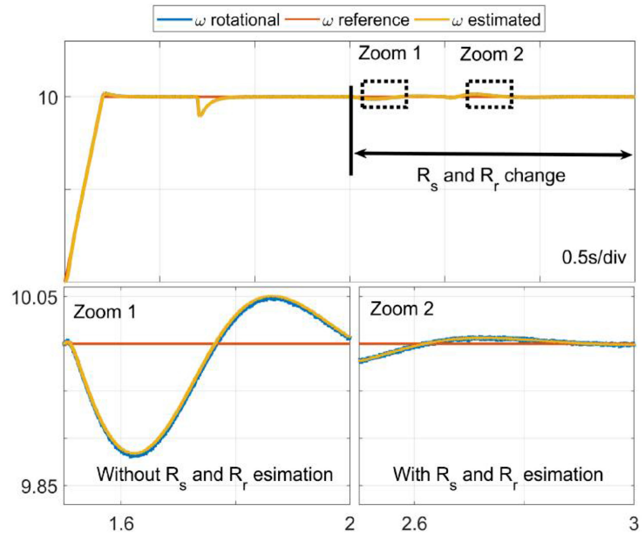

FIG. 19. The reference, rotational, and estimated speed.

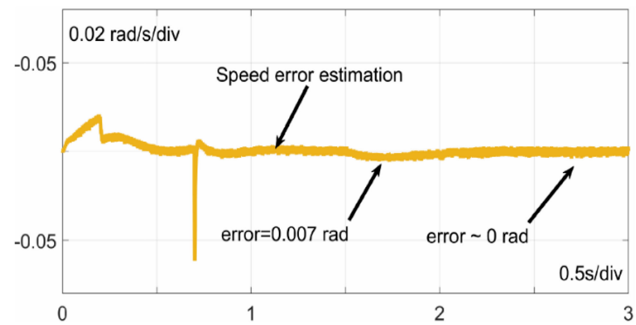

FIG. 20. The speed estimation error.

4.35 Ω, meanwhile the R_r is increased starting from 2.7 Ω until reaching 4.05 Ω at 1.5s. The proposed control and the MRAS-SM observer used the initial values of $R_s$and R_r for the entire duration. The estimated values of the $R_s$and R_r are not taken into consideration in the control during the time between 0s and 1.5s.The resistances estimation algorithm is activated at 2s to achieve better performance in the presence of parameters variations. Such test would allow for the identification of the impact of parameters variation on the proposed control. The estimated resistances are shown in Fig. 17 and Fig. 18 from which it is evident that the estimated resistances track the real values within a short time. In practice the motor parameters change slowly with temperature, which allows the estimation algorithm to identify the actual values with almost zero error.

The reference, rotational, and estimated speeds are shown in Fig. 19. It is found that the rotational speed and the estimated one follow the reference speed even at lower speeds. The estimation error is reduced from 6% to 0.2% compared to the work presented in [17]–[20], [26], [29], [38], [42], [43] and [44] as shown in Fig. 20. This result demonstrates the high performance of the proposed control technique even during relatively low speed operation in comparison to the earlier presented solutions.

The proposed control system becomes unstable during the mismatch between the real motor parameters and the values used in the controllers. The stability problem could be solved after activating the estimation algorithm of the resistances. It is clear that the estimated rotational speed becomes very close to the actual rotational speed after activating the estimation algorithm.

The observed rotor flux components indicate a good decoupling even at low-speed operation as shown in Fig 21. The developed torque presents an accurate performance and precisely tracks the load torque as shown in Fig 22. From

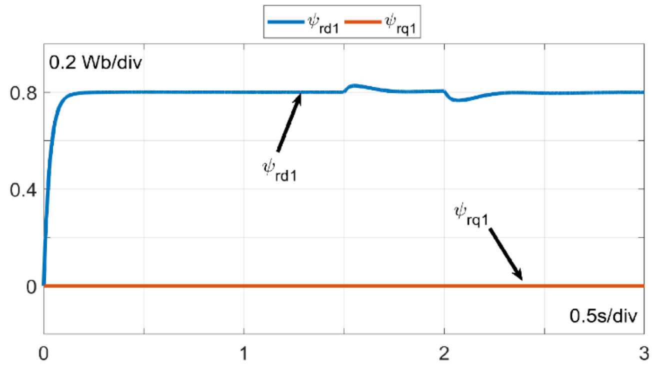

FIG. 21. **The d1-q1 rotor flux components.**

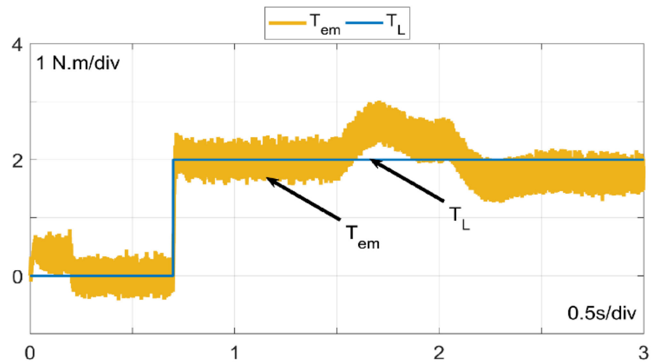

FIG. 22. **The developed electromagnetic torque with load torque disturbances.**

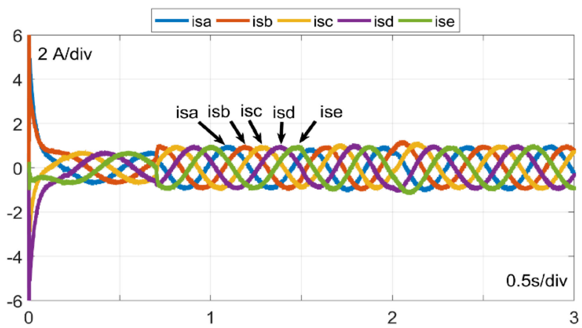

FIG. 23. **The five phase stator currents.**

Fig. 23, the five phase stator currents present sinusoidal waveforms during low-speed operation (within 10 rad/s). When R_s and R_r are changed in each phase of the studied motor, the developed electromagnetic torque is affected and the rotor flux components deviate from the reference values, which leads to a significant error in the speed estimation. The amplitudes of the five phase stator currents were changed at the instant of R_s and $R_r$variation. It is well known that the change in five phase stator currents can cause a change in d1-rotor flux and developed torque. To avoid this, the activation of the R_s and R_r estimators at 2s are performed, consequently an improved performance is obtained. The results prove that the sensorless FOC technique based on MRAS-SM observer offers improved performance and high accuracy after the activation of

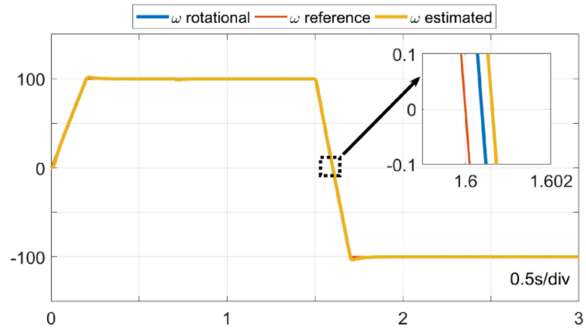

FIG. 24. **The reference, rotational, and estimated speed.**

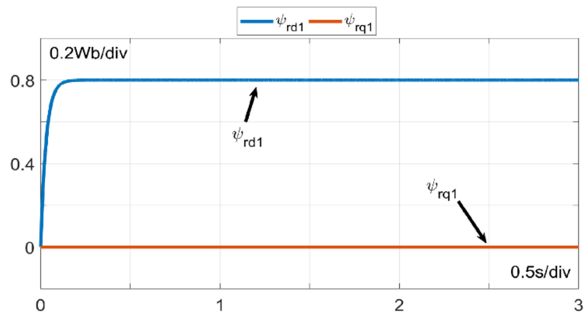

FIG. 25. **The d1-q1 rotor flux components.**

the R_s and $R_r$estimators, confirming the effectiveness of the proposed R_s and R_r estimation algorithm for the proposed sensorless control.

D. SPEED REVERSAL OPERATION

To check the effectiveness of the sensorless control under speed reverse, a special test has been performed with the estimation of the motor resistances under constant load torque. The reference speed is set at 100rad/s, and then it is decreased to reach -100rad/s at t = 1.7s. Fig. 24 shows the reference speed, the rotational speed, and the estimated speed. The rotational speed and the estimated speed converge perfectly to the reference speed during reverse operation. Fig. 25 shows the rotor flux components in the frame. It can be concluded that the d1-rotor flux component remains constant (0.8 Wb) in the whole speed range, while the q1-rotor flux component remains equal to zero.

The electromagnetic torque and the five phase stator currents under reference speed reverse are shown in Fig 26 and 27. The five phase stator currents and the electromagnetic torque, behave according to the dynamic behavior of the motor operation. On the other side, the estimated and actual motor resistances are shown in Fig. 28. The estimated R_s and R_r follow their actual values at any operating point. The step change of the speed does not affect the estimated motor resistances compared to the works presented in [19], [38].

E. INDUSTRIAL TEST TRAJECTORIES

In this section, the proposed control technique is tested according to an industrial operation profile of the studied motor

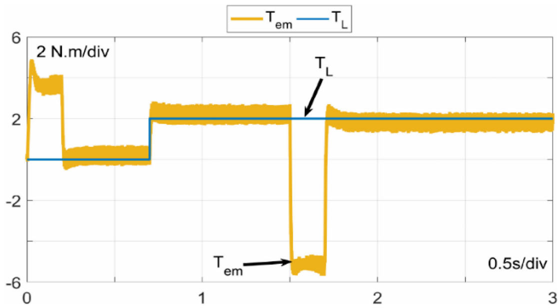

FIG. 26. The developed electromagnetic torque with load torque disturbances.

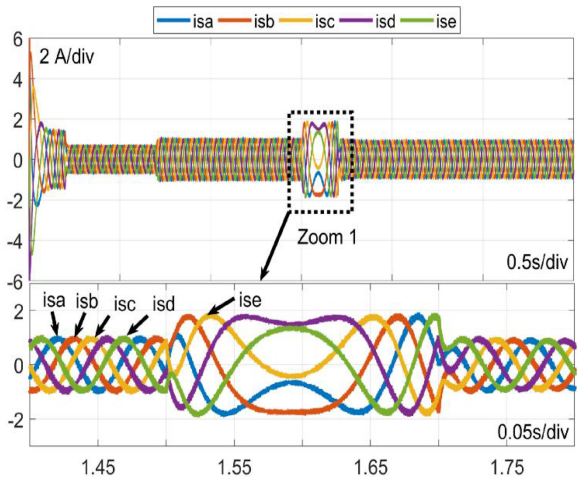

FIG. 27. The five phase stator currents.

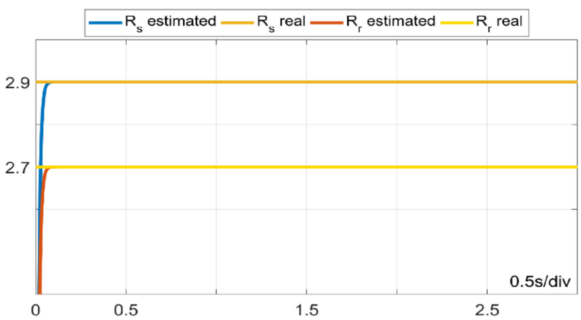

FIG. 28. The estimated resistances of rotor and stator windings.

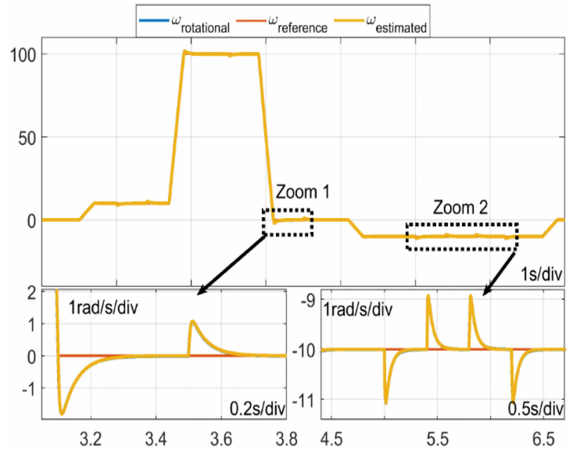

FIG. 29. The reference, rotational, and estimated speed.

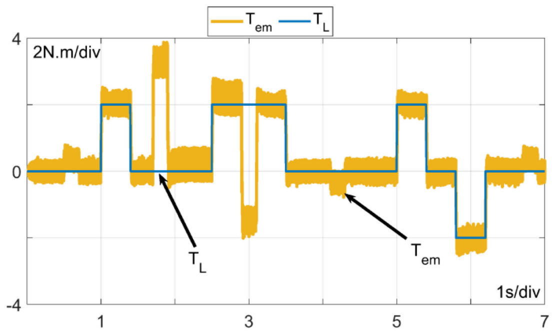

FIG. 30. The developed electromagnetic torque with load torque disturbances.

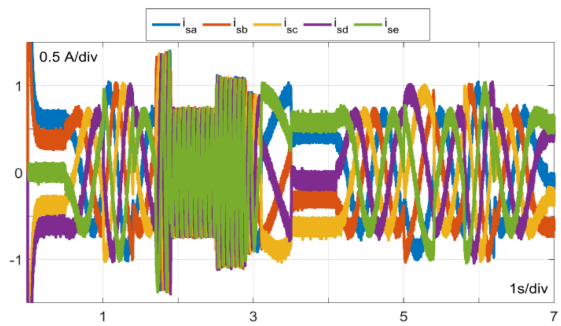

FIG. 31. The five phase stator currents.

similar to the profile presented in [45]. This profile is chosen because it contains successive scenarios within a wide range of speed variations and load torque during an interval of 7s, as shown in Fig. 29 and 30.

Fig. 29 shows that the estimated speed and the rotational one is consistent. The reference speed profile is changed within a wide range of values. The figure shows high performance operation at a relatively low speed, including zero value and reverse condition.

The load was also changed during this test. It is observed clearly from Fig. 30, a high dynamic electromagnetic torque under various operating conditions. The five phase stator currents under various test trajectories are shown in Fig. 31. Within the time interval where the speed is equal to zero, the currents behave as DC currents with different values as shown during the intervals [0s 05s], [3.1s 4.1s] and [6.9s 7s]. At the zero-speed region, the stator windings behave as a source of a nearly constant magnetic flux, which produces a fixed non-rotating torque if there is no load torque applied. However, if there is a load torque applied as in the case of the interval [3.1s 3.5s] on Fig. 30, the current's frequency becomes low initially, which is then decreased rapidly to reach zero at nearly 3.5s. It can be concluded from this test that the proposed control based on the used observers can provide high drive performance with high accuracy under different load perturbations and within a wide range of speed variations.

VI. CONCLUSION

In conclusion, a new sensorless FOC control of FPIM-OESW with dual SVM was proposed in this paper. In the proposed scheme, the MRAS-SM observer was used to ensure accurate estimation of the rotor flux and rotor speed at various operating points. Such solution ensured high estimation accuracy, implementation simplicity, and robustness against various uncertainties. The SM observer was proposed in this paper to replace the traditionally used reference model in conventional MRASs. To overcome the chattering problem related to the SM observer, a special sigmoid function was proposed to be used as the switching function. The goal is to ensure the convergence of the estimated current error to zero using a specially defined sliding surface. In addition, to minimize the influence of the load torque variation on the overall proposed control, the presented paper focused also on the estimation of the load torque. Furthermore, a simple method was proposed for the estimation of the rotor and stator resistances to ensure the speed estimation accuracy under a wide range of operation modes, particularly at low and zero speeds. The superiority and effectiveness of the proposed control technique with the proposed estimators were successfully confirmed using a hardware-in-the-loop platform under different operating conditions such as variable load torque, high/low speed operation, motor parameter changes, and speed reverse operation.

The obtained results confirm that the proposed sensorless control provides high estimation accuracy with enhanced performance under different operation conditions. The obtained results proved the effectiveness and the high accuracy of the proposed algorithm in tracking the changes of the stator and rotor resistances during motor operation compared with the previous works presented in [18]–[21], [23], [26], [27].

The proposed sensorless control using the MRAS-SM observer and parameters estimation presents a good solution for high-performance control of the multi-phase induction machine. The proposed solution does not suffer from computational complexity and can be implemented on low-cost microcontrollers. Such advantages make it a promising candidate for industrial applications.

REFERENCES

[1] I. D. Mohamed, A. E. Ahmed, M. M. Ahmed, B. Radu, and A. Shehab, "Zero-/low-speed operation of multiphase drive systems with modular multilevel converters," *IEEE Access*, vol. 7, pp. 14353–14365, Feb. 2019.

[2] A. Rosen, M. Groninger, and A. Mertens, "Modeling and optimized ¨ control of fault-tolerant H-bridge fed multiphase drives," in *Proc. 17th IEEE Eur. Conf. Power Electron. Appl.*, Sep. 2015.

[3] S. Payami, R. K.Behera, and A. Iqbal, "DTC of three-level NPC inverter fed five-phase induction motor drive with novel neutral point voltage balancing scheme," *IEEE Trans. Power Electron.*, vol. 33, no. 2, pp. 1487–1500, Feb. 2018.

[4] P. P. Rajeevan, K. Sivakumar, K. Gopakumar, C. Patel, and H. Abu-Rub, "A nine-level inverter topology for medium voltage induction motor drive with open-end stator winding," *IEEE Trans. Ind. Electron.*, vol. 60, no. 9, pp. 3627–3636, Sep. 2013.

[5] E. Levi, "Advances in converter control and innovative exploitation of additional degrees of freedom for multiphase machines," *IEEE Trans. Ind. Electron.*, vol. 63, no. 1, pp. 433–448, Jan. 2016.

[6] I. Gonzalez-Prieto, M. Duran, J. Aciego, C. Martin, and F. Barrero, "Model predictive control of six-phase induction motor drives using virtual voltage vectors," *IEEE Trans. Ind. Electron.*, vol. 65, no. 1, pp. 27–37, Jan. 2018.

[7] S. Khadar, A. Kouzou, A. Hafaifa, and A. Iqbal, "Investigation on SVM-backstepping sensorless control of five-phase open-end winding induction motor based on model reference adaptive system and parameter estimation," *Eng. Sci. Tech. Int. J.*, vol. 22, no. 4, pp. 1013–1026, Mar. 2019.

[8] M. Darijevic, M. Jones, E. Levi, A. Iqbal, and H. Abu-Rub, "Performance comparison of two four-level five-phase open-end winding drives," in *Proc. 24th IEEE Int. Symp. Ind. Electron.*, Jun. 2015, pp. 1088–1093.

[9] M. Priestley, M. Farshadnia, and J. E. Fletcher, "FOC transformation for single open-phase faults in the five-phase open-end winding topology," *IEEE Trans. Ind. Electron.*, vol. 67, no. 2, pp. 842–851, Feb. 2020.

[10] Y. Kawabata, M. Nasu, T. Nomoto, E. C. Ejiogu, and T. Kawabata, "High-efficiency and low acoustic noise drive system using open-winding AC motor and two space-vector-modulated inverters," *IEEE Trans. Ind. Electron.*, vol. 49, no. 4, pp. 783–789, Aug. 2002.

[11] B. A. Welchko and J. M. Nagashima, "The influence of topology selection on the design of EV/HEV propulsion systems," *IEEE Power Electron. Lett.*, vol. 1, no. 2, pp. 36–40, Jun. 2003.

[12] A. C. N. Maia, C. B. Jacobina, N. B. D. Freitas, and I. F. M. Pinheiro, "Open-end multilevel six-phase machine drive system with five three-leg converters," *IEEE Trans. Ind. App.*, vol. 53, no. 3, pp. 2271–2281, Jun. 2017.

[13] N. Bodo, M. Jones, and E. Lev, "A PWM method for seven- and nine-phase open-end winding motor drives," *Math. Comp. Simul.*, vol. 90, pp. 15–27, Apr. 2013.

[14] J. Listwan and K. P.´kowski, "Field-oriented control of five-phase induction motor with open-end stator winding," *Arch. Elect. Eng.*, vol. 65, no. 3, pp. 395–410, 2016.

[15] P. C. Mavila and P. P. Rajeevan, "A new direct torque control scheme for five phase open-end winding induction motor drives with reduced DC voltage requirement," in *Proc. IEEE Int. Conf. Power Electron., Smart Grid Renewable Energy*, Apr. 2020.

[16] S. Khadar, A. Kouzou, M. M. Rezaoui, and A. Hafaifa, "Fault-tolerant sensorless sliding mode control by parameters estimation of an open-end winding five-phase induction motor," *Modelling, Meas. Control*, vol. A 92, no. 2-4, pp. 6–15, 2019.

[17] E. Hamdi, T. Ramzi, I. Atif, and M. F. Mohamed, "Real time implementation of indirect rotor flux oriented control of a five-phase induction motor with novel rotor resistance adaption using sliding mode observer," *J. Franklin Inst.*, vol. 355, pp. 2112–2141, 2018.

[18] E. Hamdi, T. Ramzi, I. Atif, and M. F. Mohamed, "Adaptive direct torque control using Luenberger-sliding mode observer for online stator resistance estimation for five-phase induction motor drives," *Elect. Eng.*, vol. 100, pp. 1639–1649, 2018.

[19] T. Asghar, R. Hai-Peng, and R. Chun-Huan, "Sensorless direct torque control of the six-phase induction motor by fast reduced order extended Kalman filter," *Complexity*, 2020, Article ID 8985417.

[20] H. Abu-Rub, A. Iqbal, and J. Guzinski, "High performance control of AC drives with MATLAB/simulink, 2nd edition," *Book.*, ISBN: 978-1-119-59078-1, pp. 600, Jun. 2021.

[21] F. Bo, F. Zhumu, L. Leipo, and F. Jiangtao, "The full-order state observer speed-sensorless vector control based on parameters identification for induction motor," *Meas. Control*, vol. 52, no. 3/4, pp. 202–211, Mar. 2019.

[22] M. R. Khan and I. Atif, "Experimental investigation of five-phase induction motor drive using extended Kalman-filter," *Asian Power Electron. J.*, vol. 3, no. 1, pp. 1–7, Sep. 2009.

[23] M. Priestley, M. Farshadnia, and J. E. Fletcher, "Direct torque control of six-phase induction motor with a novel MRAS-based stator resistance estimator," *IEEE Trans. Ind. Electron.*, vol. 65, no. 10, pp. 7685–7696, Oct. 2018.

[24] B. Karanayil, M. F. Rahman, and C. Grantham, "Online stator and rotor resistance estimation scheme using artificial neural networks for vector controlled speed sensorless induction motor drive," *IEEE Trans. Ind. Electron.*, vol. 54, no. 1, pp. 167–176, Feb. 2007.

[25] R. Marino, S. Peresada, and P. Tomei, "On-line stator and rotor resistance estimation for induction motors," *IEEE Trans. Control Syst. Technol.*, vol. 8, no. 3, pp. 570–579, May 2000.

[26] M. Rashed and A. F. Stronach, "A stable back-EMF MRAS-based sensorless low-speed induction motor drive insensitive to stator resistance variation," *IEE Proc. Elect. Power Appl.*, vol. 151, no. 6, pp. 685–693, Nov. 2004.
[27] S. Maiti, C. Chakraborty, Y. Hori, and M. C. Ta, "Model reference adaptive controller-based rotor resistance and speed estimation techniques for vector controlled induction motor drive utilizing reactive power," *IEEE Trans. Ind. Electron.*, vol. 55, no. 2, pp. 594–601, Feb. 2008.
[28] H. M. Kojabadi, "Active power and MRAS based rotor resistance identification of an IM drive," *Simul. Model Pract. Theory*, vol. 17, no. 2, pp. 376–389, Feb. 2009.
[29] J. Yang, M. Dou, and D. Zhao, "Iterative sliding mode observer for sensorless control of five-phase permanent magnet synchronous motor," *Bull. Polish Acad. Sci.*, vol. 65, no. 6, pp. 845–857, 2017.
[30] K. Wubin, H. Jin, L. Bingnan, K. Min, and Z. Lihang, "Improved sliding-mode observer for sensorless control of five-phase induction motor," in *Proc. IEEE Int. Conf. Elect. Mach. Syst.*, 2013.
[31] A. Abdelkarim, K. Aissa, M. Brahim, A. Tarek, and A. Younes, "Feedback linearization based sensorless direct torque control using stator flux MRAS-sliding mode observer for induction motor drive," *ISA Trans.*, vol. 98, pp. 382–392, Mar. 2020.
[32] E. Levi, INW Nyoman, B. Nandor, and J. Martin, "A space-vector modulation scheme for multilevel open-end winding five-phase drives," *IEEE Trans. Energy Convers.*, vol. 27, no. 1, pp. 1–10, Mar. 2012.
[33] H. M. Ryu, J. H. Kim, and S. K. Sul, "Analysis of multiphase space vector pulse-width modulation based on multiple d-q spaces concept," *IEEE Trans. Power Electron.*, vol. 20, no. 6, pp. 1364–1371, Nov. 2005.
[34] S. Mohan-Krishna and J. L. Febin-Daya, "Effect of parametric variations and voltage unbalance on adaptive speed estimation schemes for speed sensorless induction motor drives,"*Int. J. Power Electron. Drive Syst.*, vol. 6, no. 1, pp. 77–85, 2015.
[35] C. Lascu, I. Boldea, and B. Frede, " Comparative study of adaptive and inherently sensorless observers for variable-speed induction-motor drives," *IEEE Trans. Ind. Electron.*, vol. 53, no. 1, pp. 57–65, Feb. 2006.
[36] N. R. Tavana and V. Dinavahi, "Real-time nonlinear magnetic equivalent circuit model of induction machine on FPGA for hardware- in-the-loop simulation," *IEEE Trans. Energy Convers.*, vol. 31, no. 2, pp. 520–530, Jun. 2016.
[37] A. Hasanzadeh, C. S. Edrington, N. Stroupe, and T. Bevis, "Real-time emulation of a high-speed microturbine permanent-magnet synchronous generator using multiplatform hardware-in-the-loop realization," *IEEE Trans. Ind. Electron.*, vol. 61, no. 6, pp. 3109–3118, Jun. 2014.
[38] T. Asghar, R. Hai-Peng, and H. H. Mohammad, "Sensorless loss model control of the six-phase induction motor in all speed range by extended Kalman filter," *IEEE Access*, vol. 8, pp. 118741–118750, Jan. 2020.
[39] N. T. Yogesh and A. V. Mohan, " Torque ripple and harmonic current reduction in a three-level inverter-fed direct-torque controlled five-phase induction motor," *IEEE Trans. Ind. Electron.*, vol. 64, no. 7, pp. 5265–5275, Jul. 2017.
[40] H. H. Mohammad, O. Mansour, and T. Asghar, "Modified DTC of a six-phase induction motor with a second-order sliding-mode MRAS-based speed estimator," *IEEE Trans. Power Electron.*, vol. 34, no. 1, pp. 600–611, Jan. 2019.
[41] G. Yiwen, L. Zou, L. Yonggang, W. Ding, G. Ruicheng, and Z. Pengfei, "Sensorless fault-tolerant control strategy of six-phase induction machine based on harmonic suppression and sliding mode observer," *IEEE Access*, vol. 7, pp. 110086–110102, Aug. 2019.
[42] L. Guohai, G. Chang, and C. Qlan, "Sensorless control for five-phase IPMSM drives by injecting HF square-wave voltage signal into third harmonic space," *IEEE Access*, vol. 8, pp. 69712–69721, Apr. 2020.
[43] P. Strankowski, J. Guzinski, M. Morawiec, A. Lewicki, and F. Wilczynski, "Sensorless five-phase induction motor drive with third harmonic injection and inverter output filter," *Bull. Polish Acad. Sci. Tech.*, vol. 68, no. 3, 2020.
[44] J. Guzinski *et al.*, " Sensorless multiscalar control of five-phase induction machine with inverter output filter," in *Proc. 19th Eur. Conf. Power Electron. Appl.*, Sept. 2017, pp. 11–14.
[45] M. A. Hamida, L. J. De, and A. Glumineau,"Experimental sensorless control for IPMSM by using integral backstepping strategy and adaptive high gain observer," *Control Eng. Pract.*, vol. 59, pp. 64–76, Feb. 2017.

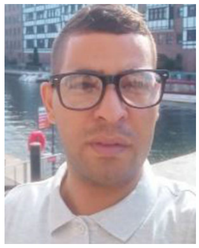

SAAD KHADAR was born in Ben Srour, Algeria, in 1992. He received the bachelor's and master's (Hons.) degrees in electrical engineering from the University of Msila, in 2011 and 2016, respectively. He is currently working toward the Ph.D. degree in engineering from the University of Djelfa, Djelfa, Algeria. In 2020, he joined Smart Grid Center Laboratory, Texas A&M University at Qatar, Doha, Qatar, as a Graduate Assistant. He has authored or coauthored more than 42 journal and conference papers. His research interests include multiphase machines and drives and on control methods in pre- and post-fault situations, power electronics devices, diagnostics and fault-tolerant control in electrical machines. He is also a Reviewer for a number of journals and conferences.

HAITHAM ABU-RUB (Fellow, IEEE) received two Ph.D. degrees. He is currently a Full Professor with Texas A&M University at Qatar, Doha, Qatar. He has research and teaching experience at many universities in many countries, including Poland, Palestine, USA, Germany, and Qatar. Since 2006, he has been with Texas A&M University at Qatar. He has served for five years as the Chair of Electrical and Computer Engineering Program with Texas A&M University at Qatar, and has been serving as the Managing Director for Smart Grid Center at the same university. He has authored or coauthored more than 450 journal and conference papers, five books, and six book chapters. He has supervised many research projects on smart grid, power electronics converters, and renewable energy systems. His main research interests include power electronic converters, renewable energy, electric drives, and smart grid. He was the recipient of many national and international awards and recognitions, including American Fulbright Scholarship and German Alexander von Humboldt Fellowship.

ABDELLAH KOUZOU (Senior Member, IEEE) was born in Djelfa, Algeria, in 1964. He is currently a Collaborator Researcher with Texas A&M University at Qatar. Since 2014, he has been the President of the Scientific Council of the Faculty. He has participated in several research projects and has led several research projects. He is the Founder of Power Electronics and Power Quality Research Group, Applied Automation and Industrial Diagnostic Laboratory, University of Djelfa. He is the Supervisor of many Ph.D. Students in Algeria. He is a Member of Smart Grid Center at Qatar SGC-Q. He is a Member of many Editorial Boards for several scientific journals and a Member of scientific and steering committees in several national and international conferences. He is the Editor-In-Chief of two journals. He is the coordinator of Algerian IEEE Power Electronics Chapter, and the Chair of sub-committee on FACTs and HVDC under the international committee PETC/IEEE-IES. He was a plenary and an Invited Keynote Speaker and Session Chair in several national and international conferences and an expert in several national and international scientific activities and project evaluations. He has authored or coauthored more than 360 papers. His main research interests include active power filtering techniques, power quality issues, power electronics devices, application of power electronics in renewable energies and application of meta-heuristics optimization algorithms, smart grid and smart buildings, reliability and diagnostics in power electronics converters.